Marine Pollution Bulletin
January 2021, Volume 162 Pages 111751 (11p.)
https://doi.org/10.1016/j.marpolbul.2020.111751
https://archimer.ifremer.fr/doc/00657/76937/

The wave regimes of the Central Pacific Ocean with a focus on pearl farming atolls

Dutheil Cyril [1, 2, 3, *] , Jullien Swen [4], Aucan J. [1], Menkes C. [1], Le Gendre Romain [5], Andréfouët S. [1]

[1] Institut de Recherche pour le Développement, UMR 9220 ENTROPIE (Institut de Recherche Pour le Développement, Université de la Réunion, Université de Nouvelle-Calédonie, Ifremer, Centre National de la Recherche Scientifique), BP A5, 98848 Nouméa Cedex, New Caledonia
[2] IRD, LOCEAN (UMR 7159), BP A5, 98848 Nouméa Cedex, New Caledonia
[3] Department of Physical Oceanography and Instrumentation, Leibniz Institute for Baltic Sea Research Warnemünde, Rostock, Germany
[4] Ifremer, Univ. Brest, CNRS, IRD, Laboratoire d'Océanographie Physique et Spatiale (LOPS), IUEM, Plouzané, France
[5] IFREMER, ENTROPIE (UMR 9220), Institut de Recherche pour le Développement, Université de la Réunion, Université de Nouvelle-Calédonie, Centre National de la Recherche Scientifique, BP 32078, 98897 Noumea Cedex, New Caledonia

* Corresponding author : Cyril Dutheil, email address : cyril.dutheil@io-warnemuende.de

Abstract :

Pearl farming sustainability in South Central Pacific (SCP) atolls strongly depends on water quality and renewal. These factors are partly controlled by the wave conditions that impact the lagoon circulation. To characterize the wave conditions around 83 SCP atolls including those hosting pearl farming activities, we used 18 years of WaveWatchIII simulation with a grid refined from 50 to 5 km resolution. Three regional wave regimes are statistically identified: two associated with long distant swells originating from mid-latitude storms, and one with local trade winds. All regimes occur with a relatively high frequency (22–44%), but with a marked seasonality. Wave conditions are also strongly modified locally during their propagation between the archipelagoes. Western and southern isolated atolls generally have a single regime all around their rims. In contrast, central Tuamotu atolls experience different regimes depending on their levels of protection. These results help understanding atoll hydrodynamics, which has implications for their management.

Highlights

► Waves are one of the main drivers of atoll lagoon circulation and larval dispersal. ► Three wave regimes are identified at day-scale based on height, direction and period. ► Wave regimes at the atoll and rim scales are identified. ► Atoll location and rim exposure strongly modify wave conditions.

Keywords : Wave regimes, Atoll hydrodynamics, Atoll rim, Tuamotu Cook Islands, WaveWatchIII

1. Introduction

Atolls are a type of coral reef formation characterized by an inside lagoon separated from the ocean by an atoll rim, which can be partly opened with passes and shallow spillways (called hoa in Polynesian, Woodroffe and .Biribo, 2011) that allow the intermittent exchange of seawater between the lagoon and the ocean. The world largest atoll-only archipelago is the Tuamotu-Gambier chain, located in French Polynesia, with 77 atolls, including 72 with lagoons (not dried or uplifted; Andréfouët and Adjeroud, 2019). Several atolls and lagoons are also present in the Society Archipelago and further west in the Cook Islands. Understanding the physical and biological functioning of their lagoons is capital for local population because marine life often provides directly or indirectly their main resources with coastal fisheries, tourism, and for many locations, black pearl farming. The latter activity is the 2nd source of income of French Polynesia, and a major activity in nearly half of the South Central Pacific (SCP) atolls.

The black pearl farming activities, namely spat collection and rearing, and their sustainability are highly dependent on water renewal and quality (Rodier et al., 2019). In addition to tide, atoll lagoon water renewal and circulation are mainly controlled by wind and wave conditions (Andréfouët et al., 2001a, 2006; Callaghan et al., 2006). Several studies have shown that wind directly influences lagoon circulation via its surface stress, while waves breaking over the reef have an indirect influence on lagoon circulation by initiating water transport from the open ocean to the lagoon through the rim (Atkinson et al., 1981; Kraines et al., 1999; Tartinville et al., 1997). These transfers depend on the geomorphology of the atoll (rim elevation, degree of aperture) but also on incident wave conditions (height, period, direction) (Andréfouët et al., 2001a; Caldwell and Aucan, 2007; Callaghan et al., 2006; Dumas et al., 2012; Hoeke et al., 2013; Tartinville and Rancher, 2000). However, little is known on the long-term wave regimes experienced by each atoll, and influencing their water quality and pearl farming potential.

Further investigations are thus warranted to enhance the characterization of the wave regimes in the SCP region, around and close to each individual atoll. Early work in the late 1990s (Young, 1999) gathered along-track altimetry data and compiled atlases. Then, Tartinville and Rancher (2000), followed by Andréfouët et al. (2001), looked at the relationship between altimetry data and flow through the atoll rims to infer the turnover time of atoll lagoons. Andréfouët et al. (2012), using 11 years of model and altimetry data, showed that events responsible for high wave height around the Tuamotu archipelago are either associated with southern swells, strong easterly winds, western local storms, or distant tropical cyclone passage, with the southern atolls of the archipelago experiencing more frequently large swells (higher than 2.5m) than the western Tuamotu atolls. Andréfouët et al., (2012) also showed that the incident waves conditions in the Tuamotu archipelago can drastically change from one atoll to another due to the shadowing effect generated by the these atolls (Chawla and Tolman, 2008; Delpey et al., 2010). Finally, Andréfouët et al. (2015) explained the occurrences of lagoon mass mortality events in the region by a combination of significant wave height, temperature and wind conditions. To go further, and understand if and how different atolls have different potential for pearl farming on the long term, it is necessary to characterize the wave climate in the region and for each individual atoll.

The present study depicts the wave regimes at multiple spatial scales around atolls, from the regional SCP scale to the atoll rim scale, by using a simulation with a multigrid approach, which allows such a downscaling. A statistical study based on k-means and hierarchical classifications is performed to robustly characterize the wave conditions, accounting not only for the wave height but also for the wave period and direction. The large-scale origin, the frequency of occurrence and the seasonal variability of regional wave regimes are computed. Along with wind regimes depicted by Dutheil et al. (2020), these results bring a new understanding of the environment of pearl farming atolls.

2. Materials and Methods

2.1 Study area

The study area is the South Central Pacific (SCP) region (130°W–165°W and 9°S–25°S; Fig. 1a, smaller box in Fig. 1b,c). The atoll scale analysis focuses on 80 sites from Tuamotu, Gambier and Society archipelagoes (all in French Polynesia), and 3 from Cook Islands. Studied sites include atolls with a central water body (true lagoon, not dry or uplifted) and two high islands (Aitutaki and Mangareva), which have been called pseudo-atolls considering their wide lagoons. For simplicity, all 83 sites will be hereafter referred as atolls. The atolls exhibit a large range of degree of closure (or aperture) to the ocean. From west to east, the density of atolls also varies significantly. The highest density of atolls, and the largest ones, are found in the central western Tuamotu (Fig. 1). Conversely, Cook Islands, East Tuamotu, and Gambier atolls are much more isolated. The most equatorial site is Manihiki in Cook Islands, the most austral sites are Mangareva and Temoe. The largest atoll in the domain is Rangiroa (1446 km^2) while the smallest studied atolls cover less than a couple of kilometer square.

2.2 Data and Modeling

- 2.2.1 Model configuration

The wave model used in the present study is the WAVEWATCH III (hereafter WW3; Tolman, 2009) spectral model version 6.07 (https://polar.ncep.noaa.gov/waves/wavewatch/). The model configuration consists of a multigrid approach with 2 two-way nested domains: a global domain at 0.5° resolution in which a first two-way nesting is performed at 0.25°, that encompasses the tropical South Pacific region (162°E-126°W; 5°N-30°S, black box in Fig. 1), and a second two-way nesting at 0.05° resolution around the atolls of interest (Fig. 1a). All grids are rectangular regular grids. The computation in the finer grid is only performed on delimited points around atolls (thanks to a masking procedure on the rectangular grid, see Fig. 1a) to limit computational cost. The open ocean points of our domain of interest masked in the 0.05° grid are thus computed on the 0.25° grid. Model bathymetry is built by interpolating at the different grid resolutions the GEBCO 30’’ bathymetry (2014 version: http://www.gebco.net/data_and_products/gridded_bathymetry_data/). In a region like French Polynesia where there is a large number of small islands and atolls, the blocking of ocean waves by these structures, too small to be resolved by a numerical grid, can be a major source of error in wave prediction models. This is why the use of an obstruction scheme is essential in this region. The obstruction scheme used here is that of Tolman (2003) which has been automated in Chawla et

Tolman (2008). From a very high resolution coastline, this scheme considers the proportion of the cell that is obscured in both x and y directions. These transparency parameters are then used as a coefficient to calculate the attenuation of the energy flow through the obscured cell. The spectral discretization (common to the 3 grids) is performed on 24 directions (15°), and 32 frequencies (from 0.0373 to 0.7159Hz with an increment factor of 1.1). The three model domains use the wave generation and dissipation parameterizations proposed by Ardhuin et al. (2010), and a third order propagation scheme (Tolman et al., 2002). Numerical schemes and parameterizations used in this configuration are summarized in Table 1. In particular, our simulations use the ST4 source term package from Ardhuin et al. (2010) with a wind-wave growth parameter, β_{max}, adjusted to 1.6, and infra-gravity waves are parameterized following Ardhuin et al. (2014). Reflection at the coast is accounted for with a coefficient of 0.1 and with a dependence to frequency.

The 10-m wind forcing field is based on the European Centre for Medium-Range Weather Forecasts fifth generation atmospheric reanalysis of the global climate, ERA5 (DOI: 10.24381/cds.adbb2d47) at 0.25° and hourly frequency. To better represent the effects of tropical cyclones, which are underestimated in this forcing, we replaced the ERA5 surface wind along tropical cyclone tracks by a statistical structure reconstructed from the observed maximum speed, retrieved in the best-tracks archive (ftp://texmex.mit.edu/pub/emanuel/HURR/tracks/). This methodology of forcing follows that of Vincent et al. (2012) and is fully detailed in Jullien et al. (*in prep.*). The ERA5 10-m wind field remains untouched out of cyclone tracks. The hindcast period for the present study covers the 2000-2017 period. January 2000 has been removed from the analysis because it is used for the spin-up period.

- 2.2.2 Data and methods for WW3 validation

The Climate Change Initiative (CCI) sea state satellite dataset (Dodet et al., 2020; Piollé et al., 2020, http://cci.esa.int/seastate) is used for validation of the modelled significant wave height (Hs). This dataset provides inter-calibrated and noise-corrected (Quilfen and Chapron, 2019) estimations of Hs from all available altimeter measurements over the period of interest. Coastal values in a 50km along-shore area flagged out because of the poor reliability of the data due to coastline interference with the signal. In order to perform an accurate comparison, the WW3 outputs are extracted along each satellite track and averaged over 0.5° grid cells to compute simulated *vs* observed significant wave height biases (Fig. 2).

2.3 Clustering methods

To identify wave regimes in the studied region**,** a statistical classification method is used to determine the main modes of wave variability during the 2000-2017 period. To that end, the daily average of the peak direction (Dp), the peak frequency (Fp) and the significant wave height (Hs) are extracted from the 18-year WW3 simulation, which amounts to 6544 days. From Dp, Fp, and Hs, three parameters are computed {Hs(t)*cos(Dp(t)), Hs(t)*sin(Dp(t)), 1/Fp(t)}, following Lecacheux et al. (2012). At each grid point, the variables are centered and reduced by subtracting the temporal mean of the whole domain and by dividing by its standard deviation. The classification by wave regimes is then performed for three different spatial scales: regional, atolls, and atoll rim sections.

At the regional scale, the 0.25° grid is used and a principal component analysis (PCA; Jolliffe, 2011) is first performed on the 6544 days of the 3 parameters {Hs(t)*cos(Dp(t)), Hs(t)*sin(Dp(t)), 1/Fp(t)}, each day being treated as an individual vector for the PCA to extract the main modes of spatial variability. The first twenty principal components are kept, representing 80% of the cumulative total variance. In that reduced space, the 6544 days are classified using a k-means classification (Diday, 1971) to determine wave regimes. This approach allows identifying wave recurrent conditions at the regional scale. One of the limitations of k-means clustering algorithms is that they require defining *a priori* the number of clusters (k), and many methods have been developed to determine the optimal number of clusters. The 'NbClust' function in factoextra R package allows comparing 26 of these methods (Charrad et al., 2014). The number of clusters kept corresponds to the most frequent between these 26 methods.

At the atoll scale, the finest 0.05° grid is used, and we define 8 geographical points (one by direction: North, North-East, East, South-East, South, Southwest, West, and Northwest) around each of the 83 atolls to extract our variables {Hs(t)*cos(Dp(t)), Hs(t)*sin(Dp(t)), 1/Fp(t)}. These points are manually pre-selected at around 8 kilometers of the atoll rim in each of the main directions (N, NE, E, SE, S, SW, W, NW), thus defining 8 domains. The exact position of these points depends also on the orientation of the atoll rim for each of these particular octants since most atolls have complex irregular shapes, and not circular shapes. Then the closest WW3 grid point is associated to the pre-defined points. For each atoll, the 3 parameters of the 8 surrounding points are concatenated and considered like one individual in the following. Then, a hierarchical classification algorithm (Euclidean distance and complete aggregation, using the ‘Cluster’ package in the R programming environment) is performed on these new 83 individuals. This approach identifies clusters of atolls that are characterized by a given wave climate around their entire periphery.

At the scale of the atoll rim geographical sectors, the same previous 8 points by atoll are considered but here each point is considered as an individual. The hierarchical classification is performed for the 664 (83*8) individual rim sections. This approach determines clusters of atoll rims characterized by a similar wave climate.

2.4 Large scale wave origins

We determine the geographical origins of the waves impacting our zone of interest by using the global wave model grid (Fig. 1b). In the open ocean, waves propagate along long circle routes or orthodromy. For each model grid point, we calculate the azimuth relative to the central point of our domain of interest (17.5°S, 144°W). Then for each grid point, the number of time steps for which the wave peak direction (Dp) is within +/- 5 degree of the target azimuth is counted. A percentage of occurrence over the entire model period (2000-2017) is then computed seasonally, and year-round. Grid points where the occurrence is lower than 2% are discarded. This simple method allows to easily visualize the areas of wave generation that will ultimately impact the targeted region. Specific work for each atoll can be conducted, but here we considered the entire region, hence the computations are made only for its center. This method does not take into account the effects of refraction, reflection or blockage by small islands.

3. Results

3.1 WW3 validation

Figure 2 displays the difference of significant wave height (Hs) between our WW3 simulation and the altimetry measurements over the 2000-2017 period. Over the global domain (Fig. 2a), WW3 simulation tends to overestimate Hs by 20 to 30 cm in the Austral Ocean and areas impacted by tropical cyclones probably because of the wind vortex interpolation on the coarse ½° induces a too wide fetch for these strong and localized events. It also underestimates Hs by 10 to 20 cm in the semi-closed seas and regions dotted with islands possibly associated to the parameterization of sub-grid scale obstructions which may be too simple. This includes the SCP region although SCP is characterized by a low bias overall (~ -5cm with few locations up to -20 or +5 cm). We also note that the bias in SCP is reduced by the higher model resolution around the atolls (not shown). Overall, these biases are relatively low and in the range of state-of-the-art wave models (Chawla et al., 2013; Rascle and Ardhuin, 2013).

3.2 Regional wave regimes

Three regional wave regimes was the consensus suggested by NbClust as the optimal number of clusters for the k-means algorithm. Figure 3 represents the temporal average of each cluster indices for the three variables (Hs, Dp, Tp=1/Fp).

3.2.1 Characteristics of the regional wave regimes

Regime 1 (R1) is a southwesterly incoming swell with a relatively high amplitude of 3.2m and a period of 14s (Fig. 3adg). The islands and atolls of the area, in particular the Tuamotu Archipelago, act as a natural barrier to this swell, strongly decreasing Hs down to 1.6m behind the denser part of the archipelago and 2.2m on the sides. The strong shadowing effect of the archipelago has the effect of rotating the mean waves direction anticlockwise and also affects the period of the swell which decreases to 13s and even less than 10 s behind the densest atoll area.

Regime 2 (R2) is characterized by south-south-east waves of 2.4m and 11.5s period (Fig. 3beh). As for Regime 1, waves are impacted when crossing the archipelago with rotation in peak direction (from 170° to 120°N) and a decrease in height and period (down to Hs<1.8m, Tp<10s) north and west of the Tuamotu.

Finally, Regime 3 (R3) is a northwesterly swell in the northern part of grid domain with a lower incoming amplitude of Hs=2.0m, and a relatively long period of more than 13s (Fig. 3cfi). In the southern part of the domain, waves come from the south-southwest (~200°N) and have a slightly shorter period (Tp<=13s) and slightly higher Hs (Hs=2.2m) than in the northern part. In this regime, the shadowing effect of the archipelago is slightly different, with a less pronounced effect on the period, which decreases from 13.5s to 12.5-13s, an anticlockwise rotation of the waves from north-west to south-west direction, and a wave height which appears relatively low all around the archipelago (Hs=1.8m). Here, the Tuamotu Archipelago has a more widespread impact on the wave height compared to its much localized effect in R1. The mean incoming direction of the waves in R1 is indeed normal to the archipelago, while in R2 the waves cross the archipelago with an angle closer to its main orientation explaining the weaker but more widespread shadowing effect. This is also associated to the two incoming wave directions: north-west in the northern part and south-south-west in the southern part of the domain.

The three regimes have different frequencies of occurrence (from 22 to 44% of the time, Table 2) with R2 being the most frequent (44.7%) following by R3 (33.3%), and R1 (22%). Their seasonal occurrence (Fig. 4) reveals that the south-southeasterly regime (R2) occur all year long but with a higher frequency in austral autumn and winter. The southwesterly and northwesterly regimes (R1 and R3) have a very strong seasonality: R1 is almost absent during austral summer, and is particularly frequent in austral winter, while R3 has an opposite behavior. This seasonality results from the wave origins.

3.2.2 Large scale wave origins

The waves impacting the SCP have different origins (Fig. 5). Incoming swells with longer periods (R1 and R3) are remotely-generated waves which originate from the mid-to-high latitudes of the northern and southern hemispheres (Fig. 5). These waves are generated by storms and therefore have a seasonal modulation, with higher occurrences during their respective winter season (Fig. 5b,c). Southern hemisphere waves impact our region all year long as shown in Fig. 4. The Austral Ocean region experiences strong winds and waves all year long, but with a stronger power in austral autumn-winter as highlighted by longer period and higher Hs in the southern part of the domain in R1 than in R3 (Fig. 3). Comparatively, northern hemisphere mid-latitude storms only occur in boreal winter (Fig. 5), and corresponding in R3 (Fig. 4) to the waves in the northern part of grid domain (Fig. 4). A third source of waves impacting our region is associated to the trade winds. These waves appear in R2 and have a seasonal distribution corresponding to the trade wind regime (see Dutheil et al. 2020). They are characterized by a shorter period associated to their more local origin. Let's note that as trade winds blow over the entire Pacific region, part of these waves can be locally generated, and part of them originate further east as shown in Fig. 5c.

3.3 Wave regimes at atoll scale

The previous section has pictured the regional pattern of wave regimes in the SCP, confirming that atolls generate or are subjected to a strong shadowing effect with very different wave conditions north and south of the Tuamotu archipelago, as well as in its different areas depending on the density, orientation, and size of atolls. Consequently, broad generalization is not granted and it appears mandatory to compute wave regimes at the atoll scale to properly assess the incoming wave conditions for each pearl farming atoll of interest.

Applying a hierarchical classification for the 83 atolls, we build the dendrogram represented in Figure 6. First, we consider 3 groups (C1, C2, C3) based on one similarity threshold, as indicated by the vertical black dashed line in Figure 6. Figure 7 shows the geographical position of the individuals of these 3 groups (green, red, and blue colors), and Table 3 their average wave characteristics. Clusters C1 and C2 have quite similar average characteristics, but the dendrogram separates these two clusters revealing that the average conditions mix different exposures to waves.

Indeed, the first cluster C1 (green) is located in the western part of the region and includes the Cook and the Society Islands (Fig. 7), and is characterized by strong exposure to northwestern and southwestern swells (R1 and R3 in Fig. 3). Cluster C2 (red, Fig. 7) groups the southeastern part of the Tuamotu atolls and the Gambier Archipelago. This cluster is more protected from the northwestern swells (R3) but exposed to the southern swells and trade winds (R1 and R2; Fig. 3). Finally, cluster C3 (blue) gathers the northern Tuamotu atolls, and appears as the less exposed cluster (mean wave height and period of 1.42m and 11.53s, Table 3). This area is indeed strongly protected for all regional regimes (see Fig. 3). It is however submitted to northwestern swells (R3 in Fig. 3) and trade winds, the latter appearing as the peak wave system for this area (Table 3, peak direction of 113.72).

The clustering structure is investigated at a second level for a lower similarity threshold that defines 13 clusters (dashed color boxes in Fig. 6). Interestingly, this new separation appears to follow very precisely the geographic limits of archipelagos and the north-south and east-west orientations for the Tuamotu Archipelago. The average characteristics of these 13 new clusters are summarized in Table 4. Cluster C1 is now divided into 3 clusters, distinguishing (Fig. 7) the northern Cook Islands (D3, green triangles), the southern Cook Islands (D2, green dot), and the Society Islands (D1, green squares). These 3 clusters slightly differ by their average conditions, notably with southern Cook Islands submitted to higher average waves but with a slightly lower period, and Society Islands showing waves with a more western peak direction than Cook Islands. This can be explained by the fact that Society Islands are exposed to less fetch during trade wind conditions, due to the protection by the Tuamotu Archipelago. Cluster C2 is split into 5 clusters separating the Gambier Archipelago (D8, red dots) showing the most energetic average wave conditions (Hs=2.05m and Tp=12.84s, Table 4) from the southern Tuamotu (D7, red squares), south-eastern Tuamotu (D4, red-crosses), and 2 clusters in the central Tuamotu (D6 red crosses, and D5 red triangles) with lower wave conditions (Hs=1.41-1.44, Table 3). All these clusters have an average south-south-west peak wave direction. Finally, cluster C3 is separated in 5 new clusters which show quite different wave conditions (Table 3). The most western cluster (D13, blue squares) is the less protected from long-incoming swell (Tp=12.19s), but acts as a strong barrier, so that cluster D10 (blue circles), west to D13, features low wave conditions (Hs=1.27m, Tp=10.52), and a north-east average peak direction. Central and most north-eastern Tuamotu (D12, D11, D10, blue square-crosses, triangle, and crosses) are relatively protected and show an average peak directions varying from south-east to east. This clustering shows an important diversity of wave conditions, especially in the central Tuamotu region depending on the atoll main exposure and on the shadowing effect by other atolls.

3.4 Wave regimes at the scale of atoll rim sections

It can be expected that rim sections with different orientations may be differently affected by waves with distinct directions and origins. To confirm this hypothesis, we finally perform a clustering on atoll rim sections (see section 2.3). The spatial distribution of the first five clusters of the dendrogram (not shown) are plotted in Figure 8.

The first cluster S1 (purple dots in Fig. 8) includes atolls from Cook Islands and Society. It occurs all around the atolls (Fig. 8abc). The second cluster S2 (green dots) gathers the rims and atolls in the south part of the study area, while S3 (blue dots) occurs in the north exposed rim sections of the Tuamotu, Society and Gambier archipelagos. Cluster S4 (red dots) and cluster S5 (yellow dots) are rarer (Fig. 8a), and located only in the northern and eastern sectors of central atolls in the Tuamotu (Fig. 8d), and Gambier (Fig. 8e). Overall, the most external parts of the study region (i.e. west, south-east and north-east) are characterized by regimes occurring all around the atolls (S1, S2 and S3 respectively), which can probably be explained by a weak protection from the other atolls and small sizes (Fig. 8abd), however, in the central part of the study area (i.e. around Tuamotu), there is a clear difference between rim sections exposed to the south-west (S2) and north-east (S3 and S4).

Table 5 provides an average description of these five regimes. S1 and S2 have close average characteristics (relatively high Hs and Tp and a south-southwestern orientation), however S1 has slightly lower Hs and Tp than S2 and a more southerly orientation. S3 and S4 shows very different characteristics than the other regimes; they are characterized by the lowest values of Hs and Tp and a north-eastern orientation. Finally, S5, which is present only at a few locations, is characterized by intermediate values of Hs and Tp and a south-east orientation.

These differences can be related to the spatial patterns of regional wave regimes, S1 being closely associated with R3 and S2 with R1. The shadowing effect in the central Tuamotu explains the low values of Hs and Tp and the north-eastern orientation of S3 and S4. S5, being present in eastern rims and characterized by an average south-eastern peak direction seems more associated with trade winds and therefore R2.

4. Discussion

Water renewal and quality are essential factors of the pearl farming production. These parameters are function of the lagoon circulation, itself controlled by environmental variables. In addition to tide, waves and surface winds conditions are major drivers of the lagoon circulation. While a better characterization of the South Pacific wind conditions is presented in Dutheil et al. (2020), the present study aims at better describing the wave conditions for the atolls of this region, specifically including pearl farming atolls. To describe the wave climate for the whole SCP region, as well as for atolls and for their rim sections, we used a WW3 simulation over the 2000-2017 period, with a nesting strategy to increase the horizontal resolution up to 0.05° around atolls, and then performed a statistical clustering of wave conditions at different scales (region, atoll, rim sections). Unlike winds which have a regional pattern not particularly affected by low-lying atoll orographic effects (Dutheil et al. 2020), waves are strongly modified when crossing the archipelagos to the point that each different atoll rim section can be exposed to specific wave conditions.

The comparison between the simulated and observed Hs only shows a slight underestimation in our study region (~0.1m), validating the relevance of our model setup for this study. We can nevertheless discuss the likely reasons for this underestimation. Tuamotu is composed of tens of atolls including several with a size smaller than 0.05° (the resolution of our finer grid). The inter-atoll distance can also be of few kilometers. These different parameters (size and distance) results in a complex topography that is not accurately captured by the interpolated bathymetry on our model grid, thus modifying the interactions (reflection, dissipation, refraction) between waves and topography. In addition, a sub-grid scale obstruction parameterization is used to represent wave dissipation by sub-grid scale atolls or islands. In the WW3 model, this parameterization is only controlled by the fraction of the sub-grid scale object compared to the cell size in the x and y directions. In addition, incident swells in the SCP are mainly SW, NW, or SSE, that is “diagonal” to the model grid cells. This might induce a lower performance of the obstruction parameterization, which is computed on the x and y sections of the grid cells. Another obstruction parameterization has been recently developed (Mentaschi et al., 2018) to circumvent this issue, but has not yet been tested in the present framework. Enhanced characterization of the obstructing factor deserves future investigation.

To characterize the wave conditions at the regional scale, we performed a k-means clustering on 3 variables. This clustering suggested 3 regional wave regimes that can be characterized notably by their directions, respectively south-westerly (R1), south-easterly (R2) and north-westerly (R3). These 3 regimes appear to have different wave origins with remote mid-latitude storm waves for R1 and R3, and a more local trade wind origin for R2. Despite the simplicity of our method to detect wave origins, there is a very good agreement with the peak direction in identified wave regimes and the detected wave origins. The only difference is in R2, which has a peak direction of 150°N in the eastern part of the domain, whereas the wave origin method points towards a 100°N origin. This difference can be explained by the clustering method, which was performed on 3 variables of equal weight and not on direction only contrary to the wave origin method. Thus, it is likely that R2 was defined by the clustering method as a regime with a short period and a low Hs, but with several wave directions including trade wind waves. This processing also explains the differences in occurrence frequency. Indeed, the wave origin method indicates a frequency of occurrence of less than 10% for waves coming from the east (Fig. 5a), whereas the frequency of occurrence of R2 is 44% (Table 2) because it probably also includes waves of other origins such as waves from the south-west and generated near the grid domain.

The results shown in Figures 6 to 8 provide new views of the different wave forcing that atolls, even geographically close, can experience. This has consequences to understand the unique behaviour of several atoll lagoons. For instance, it is known that several atolls have been more exposed to mortality events and algal blooms (Andréfouët et al., 2015). The knowledge of exposure to swell is not enough to explain alone mortality event occurrences, and it is necessary to also account for, at least, the rim geomorphology and the actual transfer of water from the ocean to the lagoon, but swell regimes are part of the lagoon vulnerability equation, and thus part of the pearl farming sustainability equation too. Figure 8 can be understood as a map of forcing potential induced by the mean incident wave conditions for each rim section. This part of the equation has now been clarified here.

The main goal of this study was to characterize the wave conditions as they are one of the major parameters controlling the lagoon circulation and thus the water quality of atolls. However, our simulation is not fine enough to compute wave transformation when approaching and entering the atoll lagoon. A transfer function evaluating how waves are transmitted into the lagoon is computed in Aucan et al. (in prep.) based on in-situ measurements. Combined with wave model results as presented here, this can be used to compute a regime of cross-reef flow to be used in hydrodynamic models of atoll lagoons (Dumas et al., 2012, Le Gendre et al, in prep.) to infer water renewal regimes.

The knowledge of the wave regime for each different rim section of the 83 atolls will also help understanding if atoll rim types, as for instance described for 16 Tuamotu atolls and their 117 rim sections in Andréfouët et al. (2001b), can be explained by present time wave conditions. A 9-

class typology of rims was computed using the surface areas of vegetation, emerged area without vegetation (carbonate conglomerate), intertidal and submerged reef flat (Andréfouët et al., 2001b). Several of the rim types were related to exposure, and the role of wave forcing in explaining the typology and the distribution of the 4 types of cover was discussed by Andréfouët et al. (2001b) but not demonstrated. With the wave data presented here, this can be now explored quantitatively, with a broader geographic scope extended to 83 atolls. Furthermore, the atoll rims dominated by emerged areas without vegetation were thought to be related to tropical cyclone occurrences in the past decades (De Scally, 2008; Laurent and Varney, 2014). Waves generated by the tropical cyclones are included in our simulation thanks to a dedicated blended forcing , future studies may thus refine a typology of atoll rims and atolls using wave and rim geomorphology data.

Finally, we did not evaluate the impact of global warming here, but it is clear that it is an important question for atoll ecosystems. To correctly and fully evaluate the impacts of future wave conditions in a global warming context, projections of surface winds and sea level rise are necessary. Reliable projections of surface winds are available for the region from Dutheil et al. (2020), whereas projections of sea level rise are still very uncertain in Earth system models with a spread ranging between 0.3 and 1m (Stocker et al., 2014). How the atoll geomorphology will be modified with by sea level rise in the future, as well as future large-scale wave conditions remain highly uncertain (McLean and Kench, 2015).

To conclude, this study provides new insights on the wave conditions at atoll scale in the south Central Pacific that could be essential for assessing the potential of pearl farming atolls, and as a first step towards the construction of an atoll typology based on location, geomorphology and wave conditions. The methodology presented here is a powerful framework for characterizing wave regimes at the atoll scale, and could finally be extended to other atolls, archipelagos and basins from the Indo-Pacific, or the Caribbean Sea.

Acknowledgements

This study was funded by the ANR-16-CE32-0004 MANA (Management of Atolls) project. The authors acknowledge the Pôle de Calcul et de Données Marines (PCDM) for providing DATARMOR storage and computational resources (http://www.ifremer.fr/pcdm). The manuscript benefited from the comments provided by two reviewers.

References

Andréfouët, S., and Adjeroud, M. (2019). French Polynesia. In World Seas: An Environmental Evaluation, (Elsevier), pp. 827–854.

Andréfouët, S., Pagès, J., and Tartinville, B. (2001a). Water renewal time for classification of atoll lagoons in the Tuamotu Archipelago (French Polynesia). Coral Reefs 20, 399–408.

Andréfouët, S., Claereboudt, M., Matsakis, P., Pagès, J., and Dufour, P. (2001b). Typology of atoll rims in Tuamotu Archipelago (French Polynesia) at landscape scale using SPOT HRV images. Int. J. Remote Sens. 22, 987–1004.

Andréfouët, S., Ouillon, S., Brinkman, R., Falter, J., Douillet, P., Wolk, F., Smith, R., Garen, P., Martinez, E., Laurent, V., et al. (2006). Review of solutions for 3D hydrodynamic modeling applied to aquaculture in South Pacific atoll lagoons. Mar. Pollut. Bull. 52, 1138–1155.

Andréfouët, S., Ardhuin, F., Queffeulou, P., and Le Gendre, R. (2012). Island shadow effects and the wave climate of the Western Tuamotu Archipelago (French Polynesia) inferred from altimetry and numerical model data. Mar. Pollut. Bull. 65, 415–424.

Andréfouët, S., Dutheil, C., Menkes, C.E., Bador, M., and Lengaigne, M. (2015). Mass mortality events in atoll lagoons: environmental control and increased future vulnerability. Glob. Change Biol. 21, 195–205.

Ardhuin, F., Rogers, E., Babanin, A.V., Filipot, J.-F., Magne, R., Roland, A., van der Westhuysen, A., Queffeulou, P., Lefevre, J.-M., Aouf, L., et al. (2010). Semiempirical Dissipation Source Functions for Ocean Waves. Part I: Definition, Calibration, and Validation. J. Phys. Oceanogr. 40, 1917–1941.

Ardhuin, F., Rawat, A., & Aucan, J. (2014). A numerical model for free infragravity waves: Definition and validation at regional and global scales. Ocean Modelling, 77, 20-32.

Atkinson, M., Smith, S.V., and Stroup, E.D. (1981). Circulation in Enewetak Atoll lagoon:. Limnol. Oceanogr. 26, 1074–1083.

Caldwell, P.C., and Aucan, J.P. (2007). An Empirical Method for Estimating Surf Heights from Deepwater Significant Wave Heights and Peak Periods in Coastal Zones with Narrow Shelves, Steep Bottom Slopes, and High Refraction. J. Coast. Res. 23, 1237.

Callaghan, D.P., Nielsen, P., Cartwright, N., Gourlay, M.R., and Baldock, T.E. (2006). Atoll lagoon flushing forced by waves. Coast. Eng. 53, 691–704.

Charrad, M., Ghazzali, N., Boiteau, V., and Niknafs, A. (2014). NbClust : An R Package for Determining the Relevant Number of Clusters in a Data Set. J. Stat. Softw. 61.

Chawla, A., and Tolman, H.L. (2008). Obstruction grids for spectral wave models. Ocean Model. 22, 12–25.

Chawla, A., Spindler, D.M., and Tolman, H.L. (2013). Validation of a thirty year wave hindcast using the Climate Forecast System Reanalysis winds. Ocean Model. 70, 189–206.

De Scally, F.A. (2008). Historical Tropical Cyclone Activity and Impacts in the Cook Islands. Pac. Sci. 62, 443–459.

Delpey, M.T., Ardhuin, F., Collard, F., and Chapron, B. (2010). Space-time structure of long ocean swell fields. J. Geophys. Res. Oceans 115.

Dodet, G., Piolle, J.-F., Quilfen, Y., Abdalla, S., Accensi, M., Ardhuin, F., Ash, E., Bidlot, J.-R., Gommenginger, C., Marechal, G., et al. (2020). The Sea State CCI dataset v1: towards a Sea State Climate Data Record based on satellite observations. Earth Syst. Sci. Data Discuss. 1–28.

Dumas, F., Le Gendre, R., Thomas, Y., and Andréfouët, S. (2012). Tidal flushing and wind driven circulation of Ahe atoll lagoon (Tuamotu Archipelago, French Polynesia) from in situ observations and numerical modelling. Mar. Pollut. Bull. 65, 425–440.

Dutheil, C., Andréfouët, S., Jullien, S., Le Gendre, R., Aucan, J., Menkes, C., 2020. Characterization of south central Pacific Ocean wind regimes in present and future climate for pearl farming application. Marine Pollution Bulletin 160, 111584. https://doi.org/10.1016/j.marpolbul.2020.111584

Diday E. (1971). Une nouvelle méthode en classification automatique et reconnaissance des formes la méthode des nuées dynamiques. Rev. Stat. Appliquée 19–33.

Hoeke, R.K., McInnes, K.L., Kruger, J.C., McNaught, R.J., Hunter, J.R., and Smithers, S.G. (2013). Widespread inundation of Pacific islands triggered by distant-source wind-waves. Glob. Planet. Change 108, 128–138.

Jolliffe, I. (2011). Principal Component Analysis. In International Encyclopedia of Statistical Science, M. Lovric, ed. (Berlin, Heidelberg: Springer Berlin Heidelberg), pp. 1094–1096.

Kraines, S.B., Suzuki, A., Yanagi, T., Isobe, M., Guo, X., and Komiyama, H. (1999). Rapid water exchange between the lagoon and the open ocean at Majuro Atoll due to wind, waves, and tide. J. Geophys. Res. Oceans 104, 15635–15653.

Laurent, V., and Varney, P. (2014). Historique des cyclones de Polynésie française: de 1831 à 2010 (Météo France, Direction interrégionale de la Polynésie française).

Lecacheux, S., Pedreros, R., Le Cozannet, G., Thiébot, J., De La Torre, Y., and Bulteau, T. (2012). A method to characterize the different extreme waves for islands exposed to various wave regimes: a case study devoted to Reunion Island. Nat. Hazards Earth Syst. Sci. 12, 2425–2437.

McLean, R., and Kench, P. (2015). Destruction or persistence of coral atoll islands in the face of 20th and 21st century sea-level rise? Wiley Interdiscip. Rev. Clim. Change 6, 445–463.

Mentaschi, L., Kakoulaki, G., Vousdoukas, M., Voukouvalas, E., Feyen, L., and Besio, G. (2018). Parameterizing unresolved obstacles with source terms in wave modeling: A real-world application. Ocean Model. 126, 77–84.

Piollé, J.-F., Dodet, G., and Quilfen, Y. (2020). ESA Sea State Climate Change Initiative (Sea_State_cci): Global remote sensing multi-mission along-track significant wave height, L2P product, version 1.1 (Centre for Environmental Data Analysis (CEDA)).

Quilfen, Y., and Chapron, B. (2019). Ocean Surface Wave-Current Signatures From Satellite Altimeter Measurements. Geophys. Res. Lett. 46, 253–261.

Rascle, N., and Ardhuin, F. (2013). A global wave parameter database for geophysical applications. Part 2: Model validation with improved source term parameterization. Ocean Model. 70, 174–188.

Rodier, M., Longo, S., Henry, K., Ung, A., Lo-Yat, A., Darius, H., Viallon, J., Beker, B., Delesalle, B., and Chinain, M. (2019). Diversity and toxic potential of algal bloom-forming species from Takaroa lagoon (Tuamotu, French Polynesia): a field and mesocosm study. Aquat. Microb. Ecol. 83, 15–34.

Stocker, T., Alexander, L., Allen, M., Independent Police Complaints Commission, IPCC, and Working Group Science (2014). Climate change 2013 the physical science basis ; Working Group I contribution to the fifth assessment report of the Intergovernmental Panel on Climate Change (Geneva: WMO, IPCC).

Tartinville, B., and Rancher, J. (2000). Wave-induced flow over Mururoa atoll reef. J. Coast. Res. 776–781.

Tartinville, B., Deleersnijder, E., and Rancher, J. (1997). The water residence time in the Mururoa atoll lagoon: sensitivity analysis of a three-dimensional model. Coral Reefs 16, 193–203.

Tolman, H.L. (2003). Treatment of unresolved islands and ice in wind wave models. Ocean Model. 5, 219–231.

Tolman, H.L. (2009). User manual and system documentation of WAVEWATCH III TM version 3.14. 220.

Tolman, H.L., Balasubramaniyan, B., Burroughs, L.D., Chalikov, D.V., Chao, Y.Y., Chen, H.S., and Gerald, V.M. (2002). Development and implementation of wind-generated ocean surface wave Modelsat NCEP. Weather Forecast. 17, 311–333.

Vincent, E.M., Lengaigne, M., Vialard, J., Madec, G., Jourdain, N.C., and Masson, S. (2012). Assessing the oceanic control on the amplitude of sea surface cooling induced by tropical cyclones: OCEANIC CONTROL OF TC-INDUCED COOLING. J. Geophys. Res. Oceans 117, n/a-n/a.

Woodroffe, C.D, Biribo, N., 2011. Atolls. In Encyclopedia of Modern Coral Reefs, Structure, Form and Process, ed. D. Hopley. pp. 51–71. Dordrecht, Netherlands: Springer Science+Business Media BV.

Young, I.R. (1999). Seasonal variability of the global ocean wind and wave climate. Int. J. Climatol. 19, 931–950.

Figure 1: Global mean of significant wave height (in m) simulated over 2000-2017 period. (a) 0.05° nested domain (blue box in b, c) in which the wave regimes are computed. (b) global 0.5° domain, (c) 0.25° nested domain (black box in b).

Figure 2: Difference of significant wave height (in m) between the WW3 simulation and the altimetry measures (from CCI sea state satellite dataset) over the different domains of simulation with different horizontal resolutions a) 0.5°, b) 0.25° and c) 0.05°. The comparison is based on the collocation between the altimetry measurements and the data modeled on a 0.5° grid. Note the color-scale is refined for panel c.

Figure 3: Composite maps showing the temporal average of the three main regional wave regimes over the period 2000-2017. These regimes are computed on 0.25° grid and on [130°W–165°W ; 9°S–25°S] domain.

Figure 4: Monthly mean occurrence (in number of days per month) of the three main regional waves regimes.

Figure 5: Percentage of occurrence of waves reaching the central point of the SCP region (16°S, 142°W within +/-5° of the great circle route azimuth), (a) year-round, (b) in December-January-February (DFJ), and (c) in June-July-August (JJA).

Figure 6: Cluster dendrogram classifying the wave characteristics (Hs, Dp, Tp) of 83 South Pacific atolls. Green (C1), red (C2), and blue (C3) colors denote the 3 first clusters. Then the second level of clusters is also identified with dashed boxes and symbols (also pictured in Fig. 7).

Figure 7: Map representing the spatial distribution in SCP of 13 wave clusters (as identified in Fig. 6). As denoted in Fig. 6 colors represent the first level of clustering, and symbols the second level. Black ellipses qualitatively indicate the main archipelagoes.

Figure 8: Map representing the spatial distribution of the first 5 clusters characterizing the wave conditions at the atoll rim scale. Color dots differentiate the clusters (S1: purple, S2: green, S3: blue, S4: red, S5, orange). (a) shows the whole SCP area of interest, (b-e) are zooms on (b) the Northern Cook Islands, (c) the Society, (d) the Gambier, and (e) the Tuamotu archipelagoes

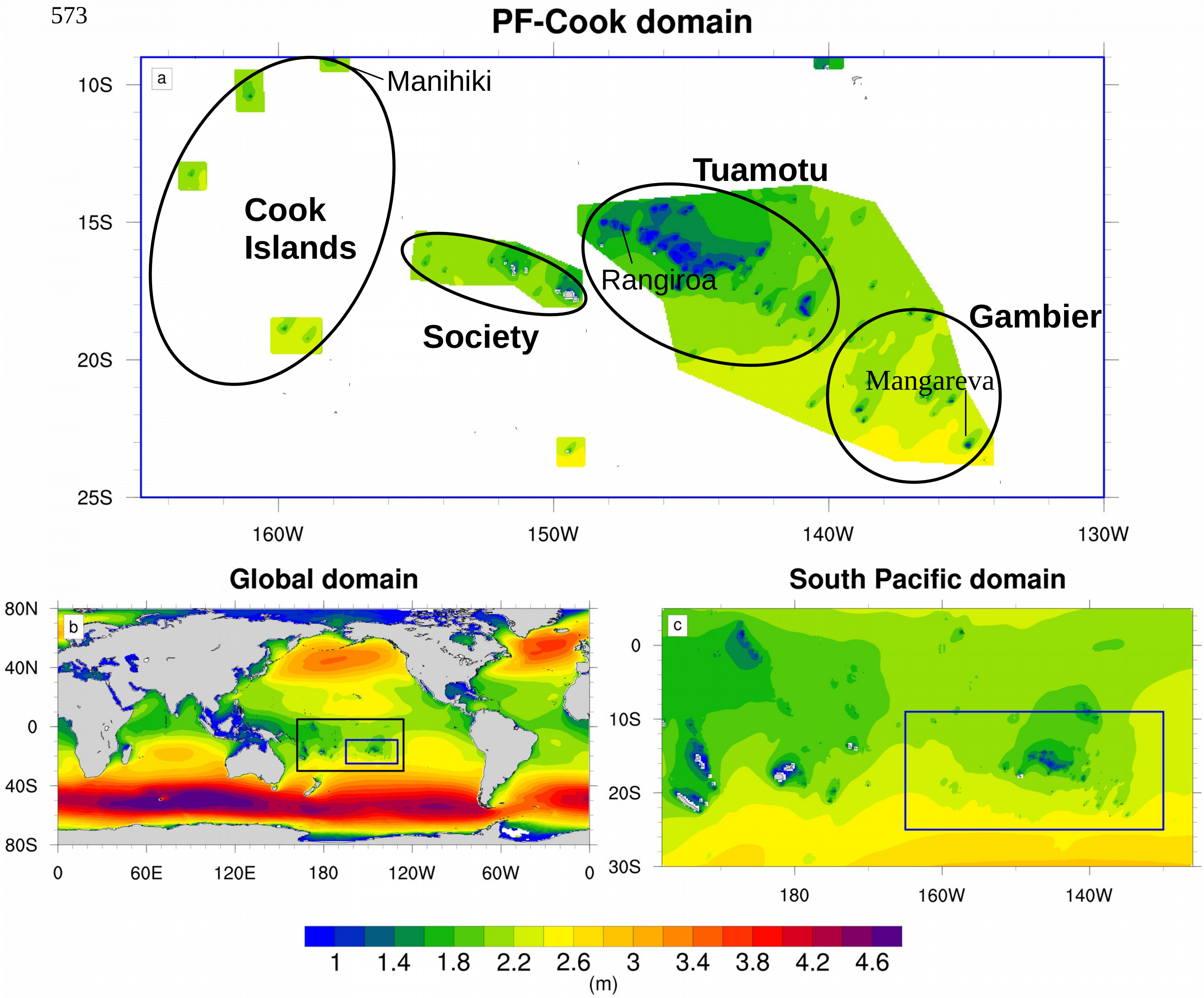
PF-Cook domain
a
Manihiki
Cook Islands
Society
Tuamotu
Rangiroa
Gambier
Mangareva
10S
15S
20S
25S
160W
150W
140W
130W
Global domain
b
80N
40N
0
40S
80S
0
60E
120E
180
120W
60W
0
South Pacific domain
c
0
10S
20S
30S
180
160W
140W
1
1.4
1.8
2.2
2.6
3
3.4
3.8
4.2
4.6
(m)

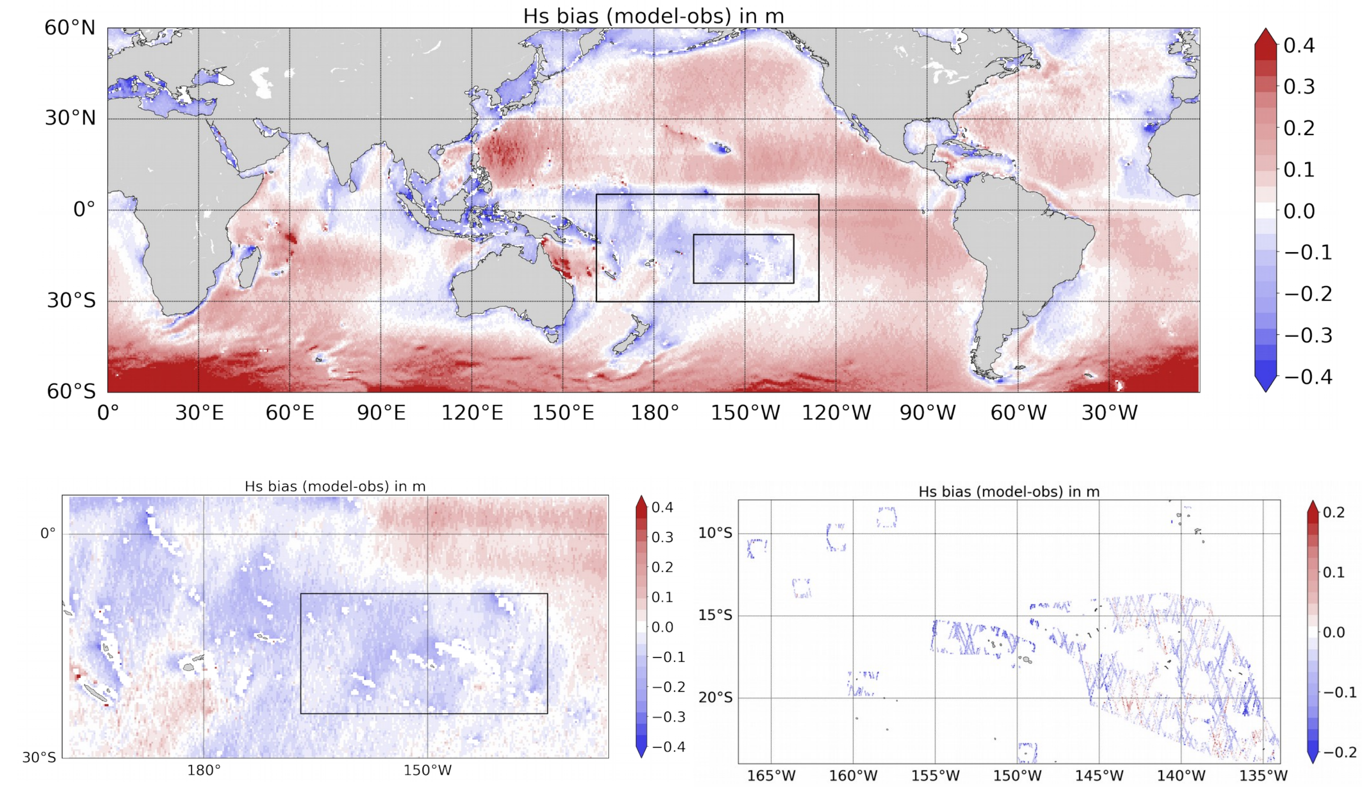

Hs bias (model-obs) in m
60°N
30°N
0°
30°S
60°S
0°
30°E
60°E
90°E
120°E
150°E
180°
150°W
120°W
90°W
60°W
30°W
0.4
0.3
0.2
0.1
0.0
−0.1
−0.2
−0.3
−0.4
Hs bias (model-obs) in m
0°
30°S
180°
150°W
0.4
0.3
0.2
0.1
0.0
−0.1
−0.2
−0.3
−0.4
Hs bias (model-obs) in m
10°S
15°S
20°S
165°W
160°W
155°W
150°W
145°W
140°W
135°W
0.2
0.1
0.0
−0.1
−0.2

Figure 2

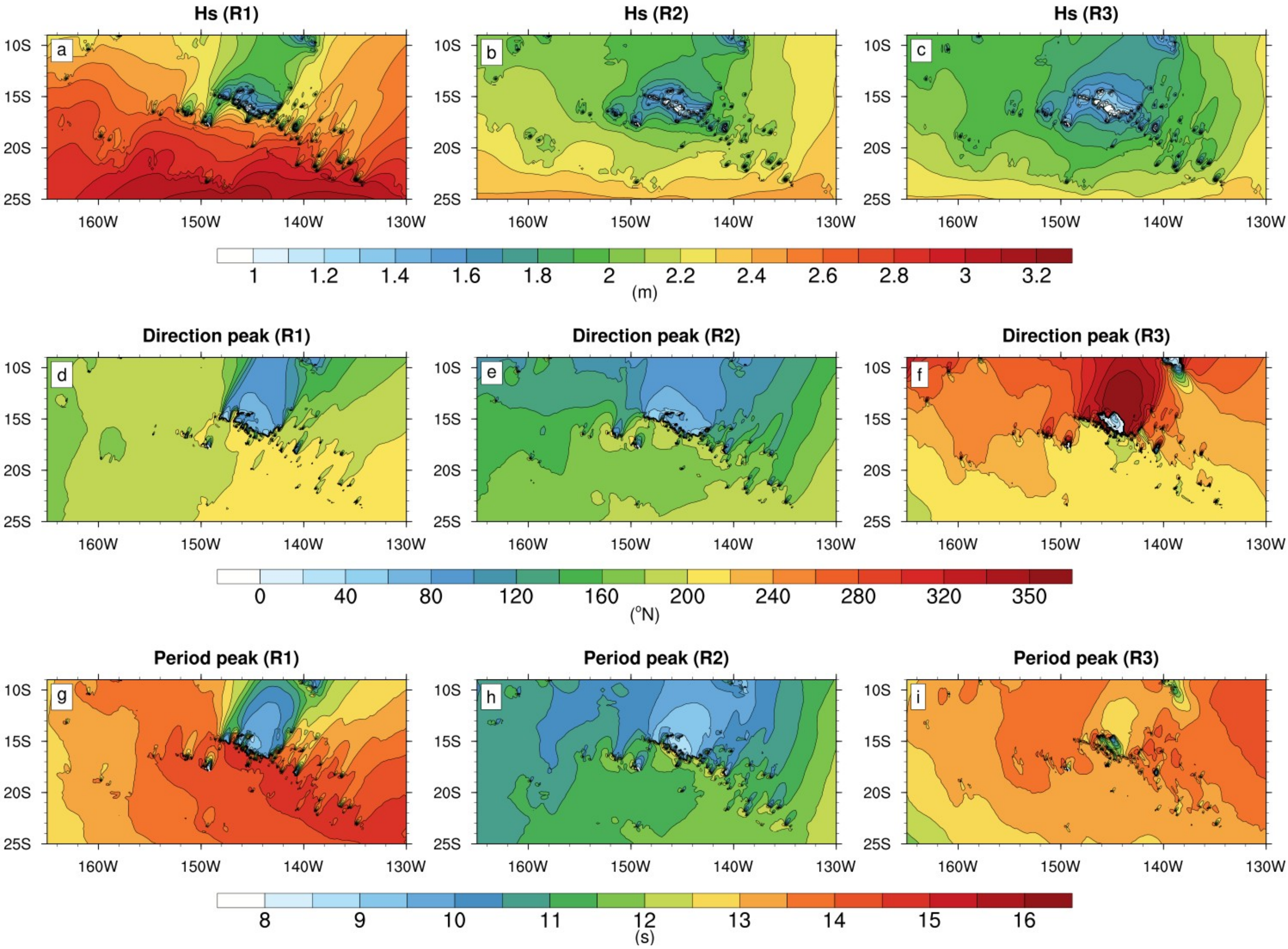
Hs (R1)
Hs (R2)
Hs (R3)
a
b
c
10S
15S
20S
25S
160W
150W
140W
130W
1
1.2
1.4
1.6
1.8
2
2.2
2.4
2.6
2.8
3
3.2
(m)
Direction peak (R1)
Direction peak (R2)
Direction peak (R3)
d
e
f
0
40
80
120
160
200
240
280
320
350
(°N)
Period peak (R1)
Period peak (R2)
Period peak (R3)
g
h
i
8
9
10
11
12
13
14
15
16
(s)

Figure 3

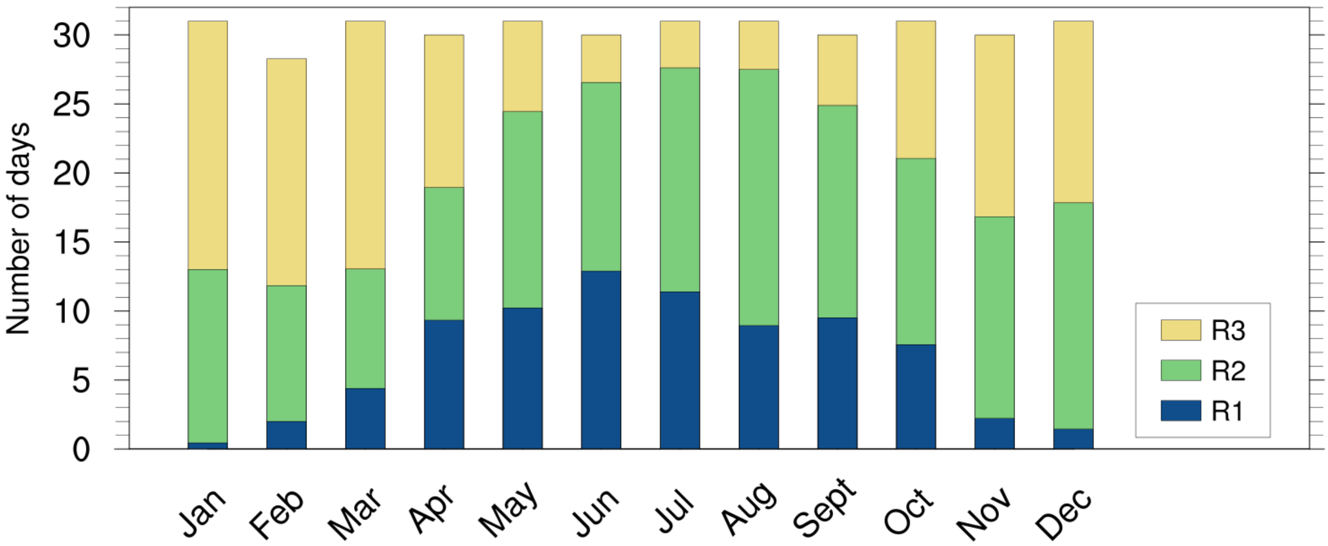
Number of days
0
5
10
15
20
25
30
Jan
Feb
Mar
Apr
May
Jun
Jul
Aug
Sept
Oct
Nov
Dec
R3
R2
R1

Figure 4

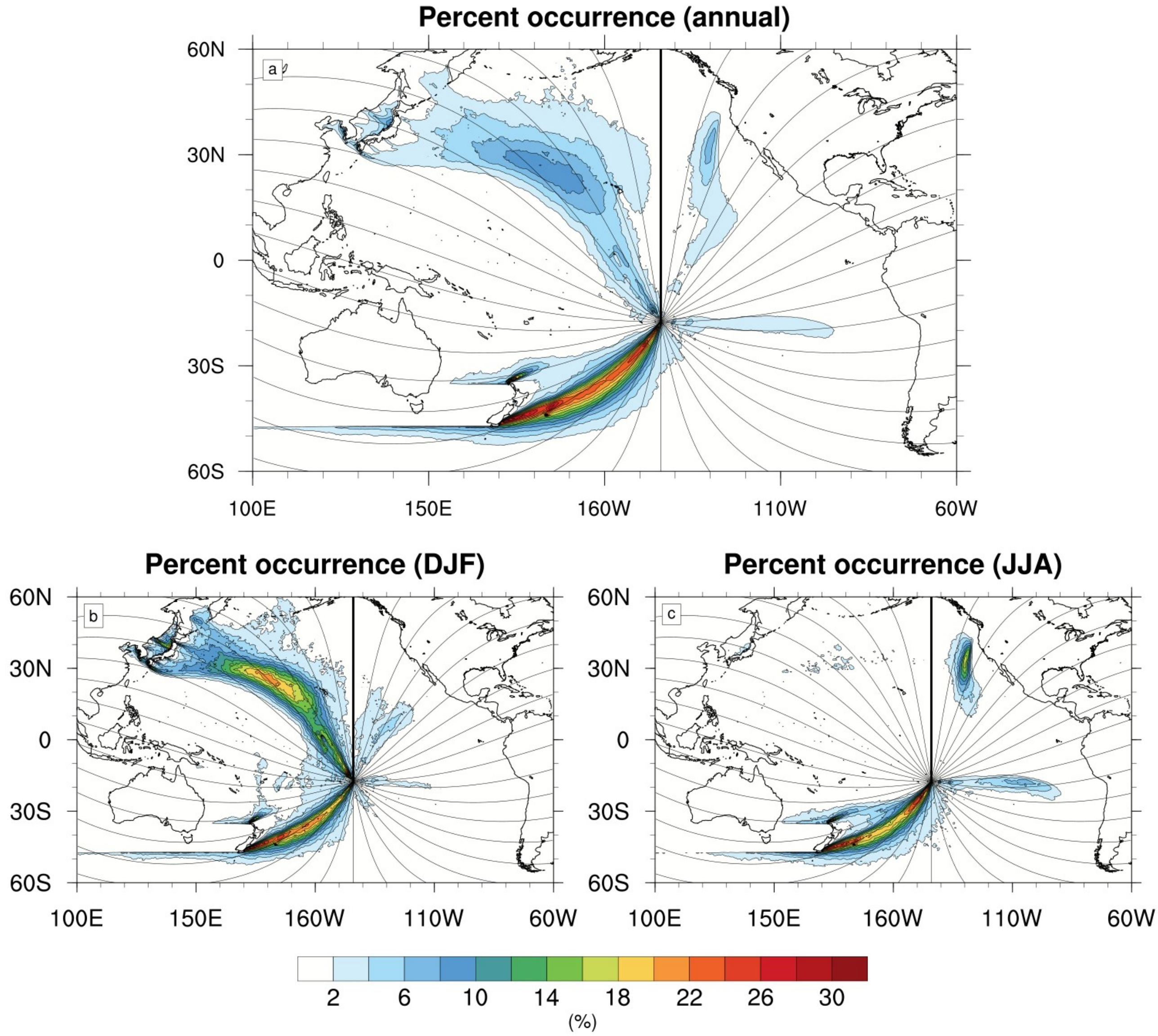
Percent occurrence (annual)
a
60N
30N
0
30S
60S
100E
150E
160W
110W
60W
Percent occurrence (DJF)
b
Percent occurrence (JJA)
c
2
6
10
14
18
22
26
30
(%)

Figure 5

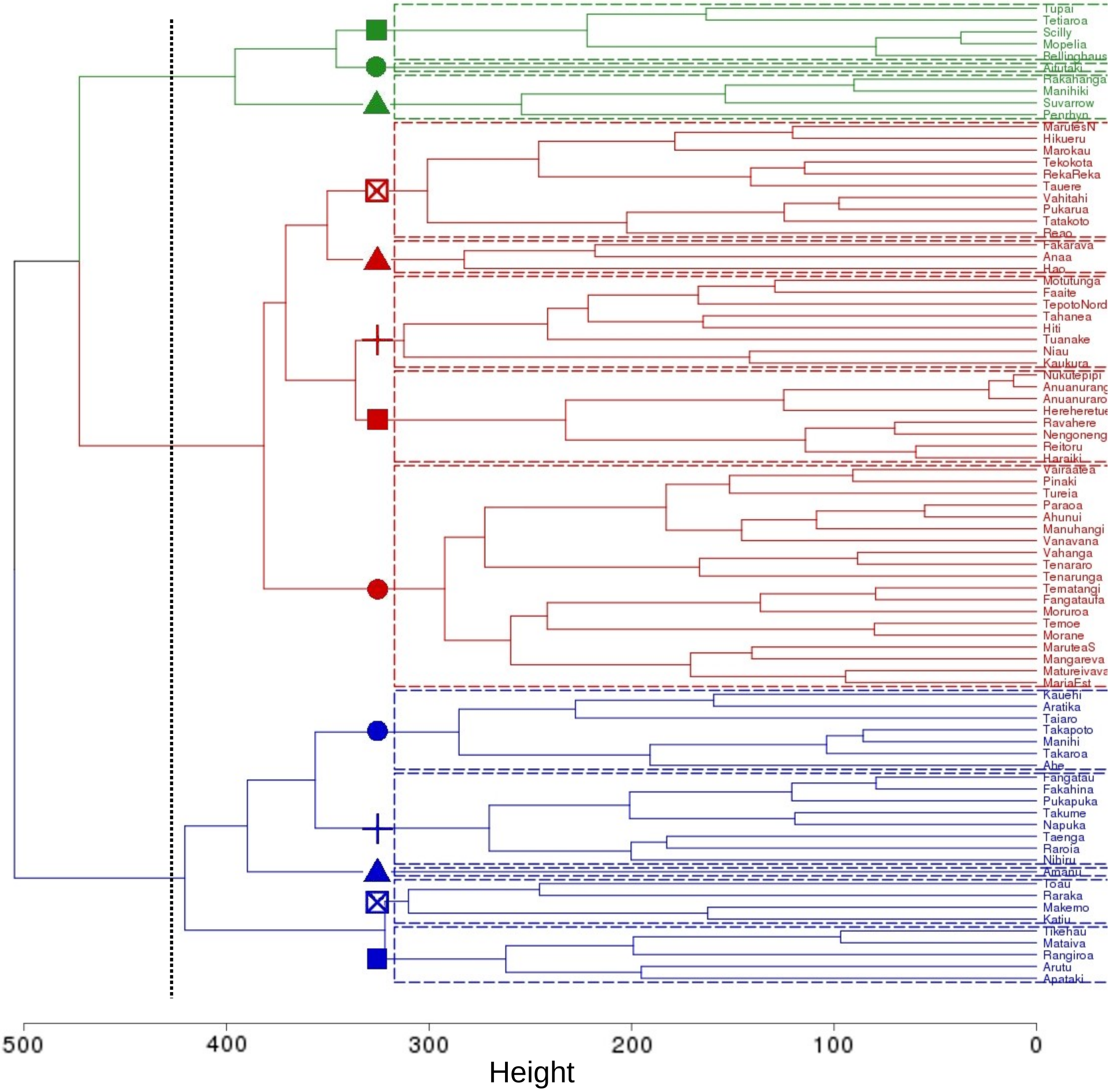
Tupai
Tetiaroa
Scilly
Mopelia
Bellinghaus
Aitutaki
Rakahanga
Manihiki
Suvarrow
Penrhyn
MarutesN
Hikueru
Marokau
Tekokota
RekaReka
Tauere
Vahitahi
Pukarua
Tatakoto
Reao
Fakarava
Anaa
Hao
Motutunga
Faaite
TepotoNord
Tahanea
Hiti
Tuanake
Niau
Kaukura
Nukutepipi
Anuanurang
Anuanuraro
Hereheretue
Ravahere
Nengoneng
Reitoru
Haraiki
Vairaatea
Pinaki
Tureia
Paraoa
Ahunui
Manuhangi
Vanavana
Vahanga
Tenararo
Tenarunga
Tematangi
Fangataufa
Moruroa
Temoe
Morane
MaruteaS
Mangareva
Matureivava
MariaEst
Kauehi
Aratika
Taiaro
Takapoto
Manihi
Takaroa
Ahe
Fangatau
Fakahina
Pukapuka
Takume
Napuka
Taenga
Raroia
Nihiru
Amanu
Toau
Raraka
Makemo
Katiu
Tikehau
Mataiva
Rangiroa
Arutu
Apataki
500
400
300
200
100
0
Height

Figure 6

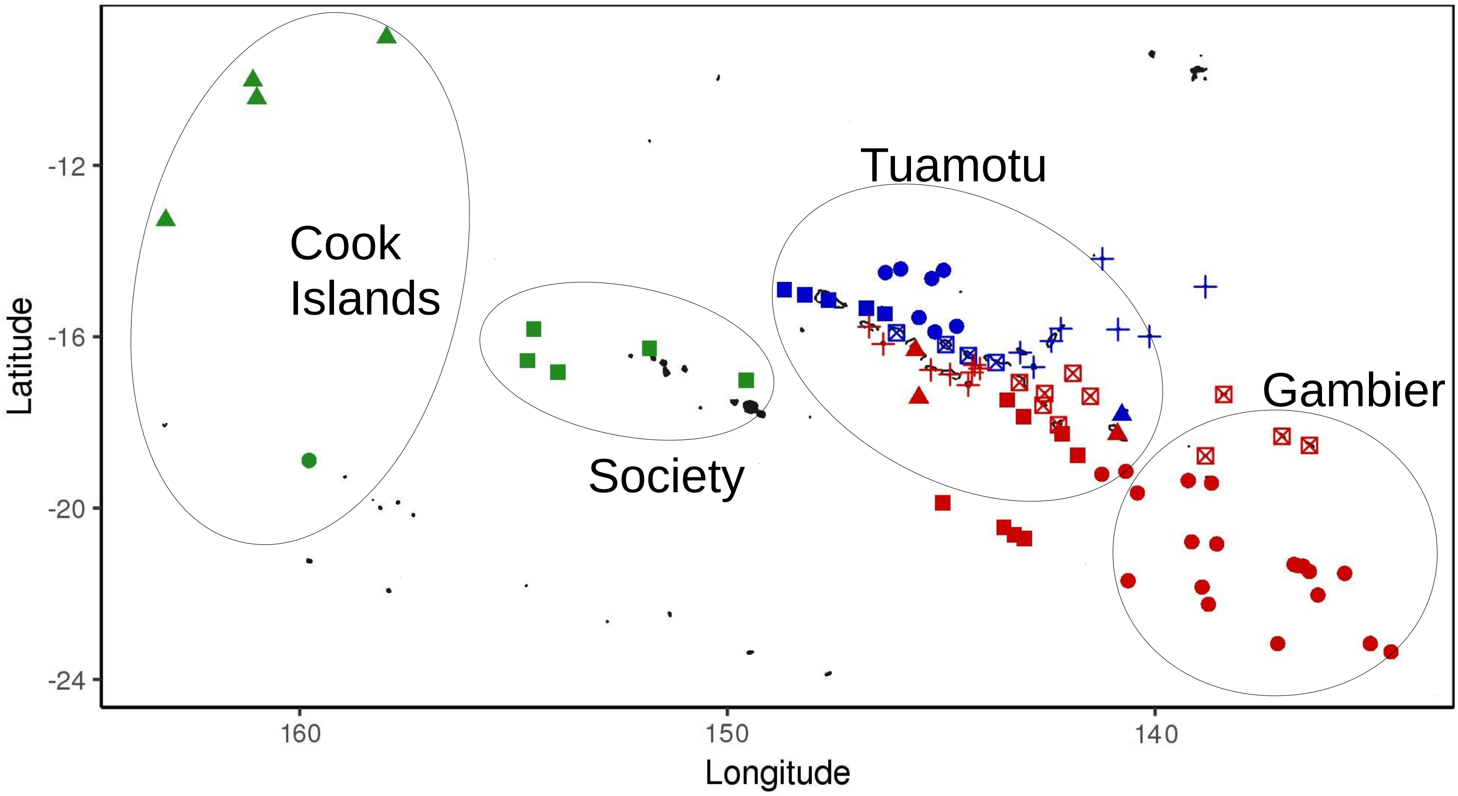

Tuamotu
Cook
Islands
Society
Gambier
-12
-16
-20
-24
Latitude
160
150
140
Longitude

579 **Figure 7**

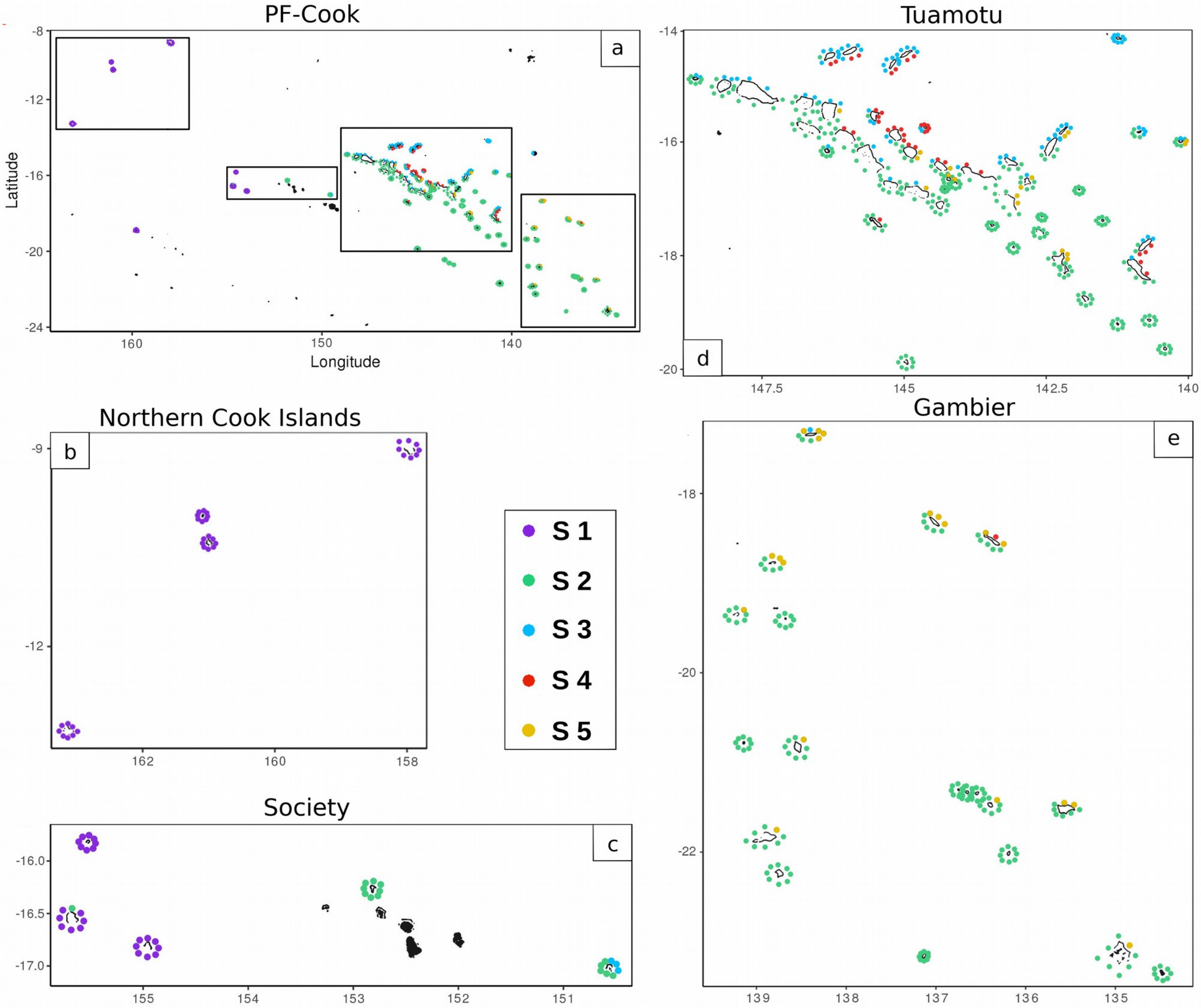

PF-Cook
a
Latitude
Longitude
Tuamotu
d
Northern Cook Islands
b
S 1
S 2
S 3
S 4
S 5
Society
c
Gambier
e

580 **Figure 8**

Table 1: Numerical schemes and parameterizations used in this WW3 configuration.

WW3 switch	Description	Parameters
PR3 UQ	Ultimate Quickest third order propagation scheme (Tolman 2002)	Default values
LN1	Cavaleri and Malanotte-Rizzoli (1981) linear source term	Default values
ST4 FLX0 STAB0	Ardhuin et al. (2010) source term package	FXFM3 =2.50 BETAMAX = 1.60000 TAUWSHELTER = 0.30000 SWELLF = 0.69000 SWELLF3 = 0.02200 SWELLF4 = 150000.0 SWELLF7 = 468000.00
NL1	Non-linear wave-wave interactions modelled using the discrete interaction approximation of Hasselmann et al. (1985)	Default values
BT4	SHOWEX bottom friction (Ardhuin et al. 2003)	Default values
DB1 MLIM	Depth-induced breaking (Battjes and Janssen 1978) with a Miche-style shallow water limiter for maximum energy	Default values
REF1	Reflection at the coast	REFCOAST = 0.10 REFFREQ = 1.00
IG1	Infra-gravity waves	IGMETHOD = 2 IGADDOUTP = 0 IGSOURCE = 2 IGSTERMS = 0 IGBCOVERWRITE = T IGSWELLMAX = T IGMAXFREQ =0.0300 IGSOURCEATBP = 0 IGKDMIN = 1.1000 IGFIXEDDEPTH = 0.00 IGEMPIRICAL = 0.001250

Table 2: Spatial average characteristics of the three regional wave regimes.

	Frequency	Hs (in m)	Dp (in °N)	Tp (in s)
Regime 1	1446 (22%)	2.5	190.0	13.4
Regime 2	2938 (44.7%)	2.1	157.7	10.9
Regime 3	2191 (33.3%)	2.0	235.0	13.4

Table 3: Average characteristics of the three main wave regimes at atoll scale

	Hs (m)	Tp (s)	Dp (°N)
C1	1.82	12.34	194.07
C2	1.87	12.67	195.00
C3	1.42	11.53	113.72

Table 4: Average characteristics of the thirteen main wave regimes at atoll scale

	Hs (m)	Tp (s)	Dp (°N)
D1 (green squares)	1.80	12.46	203.38
D2 (green circles)	1.97	12.08	185.80
D3 (green triangles)	1.82	12.25	181.17
D4 (red square-cross)	1.81	12.49	190.58
D5 (red triangles)	1.44	12.00	184.77
D6 (red cross)	1.41	12.59	190.75
D7 (red squares)	2.05	12.80	196.20
D8 (red circles)	2.05	12.84	199.53
D9 (blue circles)	1.27	10.52	46.86
D10 (blue cross)	1.66	11.97	158.90
D11 (blue triangles)	1.32	11.00	91.19
D12 (blue square-cross)	1.25	11.72	163.17
D13 (blue squares)	1.40	12.19	198.02

Table 5: Average characteristics of the five first wave regimes at the scale of atoll rim sections

	Hs (m)	Tp (s)	Dp (°N)
S1	1.81	12.30	188.26
S2	1.82	12.81	198.11
S3	1.40	11.29	41.13
S4	1.28	9.44	65.30
S5	1.68	11.55	145.41